KMITL Sci. Tech. J. Vol. 16 No. 1 Jan-Jun. 2016

Microstructural Effects of Pre-aged Stainless Steels on Carbon Nanotubes Growth

Napat Kiatkangvanklai[1], Winadda Wongwiriyapan[2], Kritapas Laohhasurayotin[3] and Panya Kansuwan[1*]

[1*]Department of Mechanical Engineering, Faculty of Engineer, King Mongkut's Institute of Technology Ladkrabang, Bangkok, Thailand
[2]College of Nanotechnology, King Mongkut's Institute of Technology Ladkrabang, Bangkok, Thailand
[3]National Nanotechnology Center, National Science and Technology Development Agency, Pathumthani, Thailand

Abstract

Catalytic roles of precipitates inside the 316L stainless steel (SS) were investigated on four distinct microstructures of substrates which were prepared according to suggesting aging time and temperature in published time-temperature-precipitate (TTP) diagrams. Standard metallographic process of polishing and etching were preformed to verify attained particular inclusion types and distributions on the substrates where the chemical vapor decomposition of a mixture of alcohol vapor and Ar gas took place. After the decomposition, carbonaceous materials had grown allowing us to examine surface morphology by scanning electron microscope (SEM). The results revealed bundles of carbon nanotubes (CNTs) found along grain boundaries (GBs) where carbide phase of type $M_{23}C_6$ favorably precipitated. This indicated active catalytic types of the carbide for ethanol decomposition reaction. Uniform growth of CNTs was expected if uniform microstructures of distributed finer carbides could be established on the metallic substrates. Nevertheless, higher aging temperature coarsened carbide precipitates while accelerated intermetallic phase formation inside the steel matrix. Different morphology of carbon deposits was observed on the steel; thus, altering CNTs formation mechanism was altered upon the present of the intermetallic σ-phase.

Keywords: Carbon nanotubes, Chemical vapor deposition, Ethanol vapor, Stainless steels, 316L

1. Introduction

CNT synthesis techniques can be classified by carbon source phases: solid and gas. A decomposition of the carbon source into elemental carbon atoms occurs on specific catalytic particles where either a thermodynamically stable or metastable form precipitates. Nanotube is one of the allotropic atomic rearrangements when low O_2 partial pressure environment is fulfilled at an enough elevated temperature. Among various contemporary CNT manufacturing methods, the arc discharge or laser ablation processes using graphite rods as solid carbon source here in containing catalyst particles could produce selective CNTs with less structural defects [1]. Nonetheless, no advantage would be gained if the yields could not be assembled into a practical structure. Chemical vapor deposition (CVD) method is thus an uprising solution since not only can CNTs be

[*]Corresponding author: E-mail: panya.ka@kmitl.ac.th

synthesized but also structurally implanted on the patterned substrates. Such a structure, i.e. hybrid nano-metallic materials, has shown excellent characteristics to fabricate field electron emitters in cold cathode devices [2] and electrodes in supercapacitors [3].

The applications in the realms of field emission devices and supercapacitors prefer arrays of aligned CNTs on metallic substrates with a satisfactory level of electrical conductivity and mechanical bonding of CNTs to the substrates. This however is less likely achievable without sophisticates manufacturing techniques. To diminish the laborious task, catalyst particles should be embedded onto the substrate surface, giving rise to the direct growth methods on Fe-Ni-Cr alloy substrates [4-6]. Among these researches, Ghoebani *et al*. [5] and Camilli *et al*. [6] reported catalytic types of metal-containing particles inside CNTs using the energy dispersive X-ray spectroscopy technique (EDX) inside transmission electron microscopes.

Of particular importance in our research are the types of the particles detected and those which are already predominant in SSs. If this is the case, size and distribution of pre-existed precipitates would inevitably influence the synthesis of CNTs and, as a result, their morphology. Since type, size, and distribution of precipitates designate microstructure of steel, varying the characters results in countless steel microstructure. Despite the mirage of the steel microstructures simulated by heat treatment, there exists no study on catalytic behaviors of the pre-existent particles that could alter CNT formation mechanisms. The objective of this research is thus to present the preliminary findings on the correlation between pre-aged SS microstructure of grade 316L, as defined by aged time and temperature, and the morphology of synthesized carbonaceous deposits.

2. Experimental Procedures

2.1 Distinct Pre-aged Microstructure Preparation

Cylindrical sections of 30 mm height were cut from 316L austenitic SS rods with diameter 25 mm. chemical compositions of the steel in wt% are C-0.030, Cr-16.910, Ni-10.133, Mo-2.166, Mn-1.578, Si-0.273, P-0.027, S-0.020, and Fe-balance. Due to known former pretreated condition, the specimens were firstly solution treated at 1200°C for an hour to establish carbide-free microstructure which was preserved after water-quenched (WQ). The as-quenched microstructure was thermodynamically unstable and amenable to change when exposed to an elevated temperature. Published TTP diagrams [9] were consulted for four set of time-temperature parameters to produce four substrates with different microstructures. Figure 1 summaries the heat treatment conditions for each sample namely A, B, C, and D. Microscopic methods with assisted hardness measurement were used to characterize the microstructures of the samples. Precipitates at particular interesting locations were analyzed compositionally by EDX.

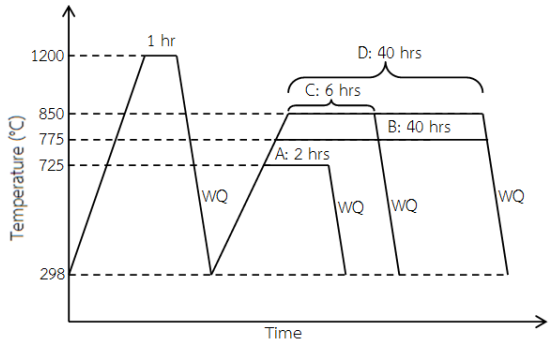

Figure 1. Heat treatment procedures of sample A, B, C, and D.

2.2 CNT Synthesis by CVD using Ethanol as the Carbon Source

Metallographic samples were prepared by standard methodology. After 1200 mesh grinding, diamond suspension with particle size 6, 3, and 1 μm was used successively to produce mirror-like surfaces. The samples were ultrasonically cleaned in acetone for 30 s and subsequently blew dried in jet air. During the process, oxide film had developed to cover the surfaces. To diminish complex influence of the film on our experiments, the film was usually reduced by prolonging the samples at an elevated temperature under inert gas atmosphere. Ar gas was the simplest choice which was feed at the rate of 500 sccm to treat them while placed at middle zone of a furnace. After 10 min, surfaces were replenished ready for CVD process. This commenced upon increasing the gas flow of 1000 sccm through a heating flask inside which ethanol stayed at its boiling point (about 80°C). The synthesis lasted 20 min before the furnace was shut down and the ethanol gas line was closes. Afterward, Ar was maintained at 500 sccm to cool the samples down to 300°C and to room temperature in still air. The process diagram is demonstrated in Figure 2 according with experimental equipment in Figure 3. Morphology of carbon deposits were investigated by SEM; Zeiss modal Evo MA10. Comparison the morphologic appearance with metallographic and EDX results was established to assess the influence of initial SS microstructure on the synthesis of CNTs.

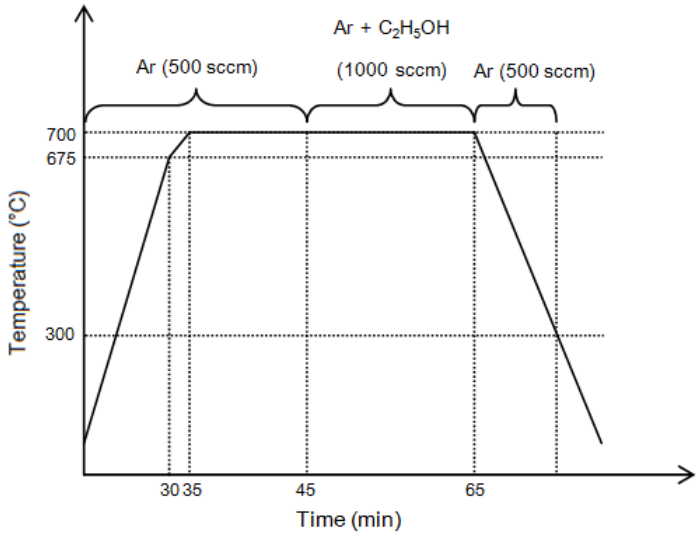

Figure 2. CVD processing time-temperature diagram.

3. Results and Discussion

3.1 Characterization of Pre-aged Microstructures

As-quenched microstructures after solution treated at 1200°C for 1 h are presented in Fig.4. When viewed in planes parallel to a deforming axis of the rods the inclusions were found elongated and aligned (Figure 4(a)) but appeared globular in planes perpendicular to the axis (Figure 4(b)). Since the experimental steels are of general application, poor cleanliness expresses high content of remained nonmetallic inclusions. Among various types of nonmetallic inclusions, oxide and sulfide are the major indigenous inclusion when solute elements exceed their solubility limit in steels. Basic discrimination between the inclusions was partly conducted according to microscopic test

methods [7]. The morphologic investigation assigned most of the inclusions found in the samples to an oxide-type category. They usually are complex oxides types such as $NiMnO_3$ and $(Ni,Zn)Fe_2O_4$ instead of simple ones, e.g. FeO, MnO, Cr_2O, TiO_2, etc [8]. Certainly, microanalytical techniques for chemical composition such as EDX after bulk extraction methods should be performed for more specific identification.

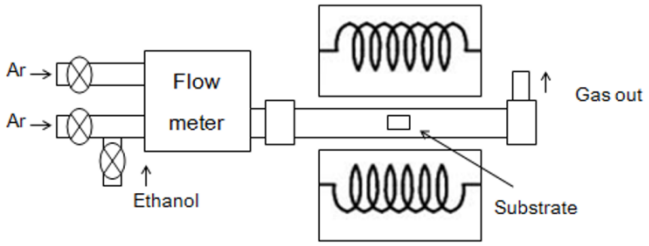

Figure 3. Schematic diagram of the reactor components.

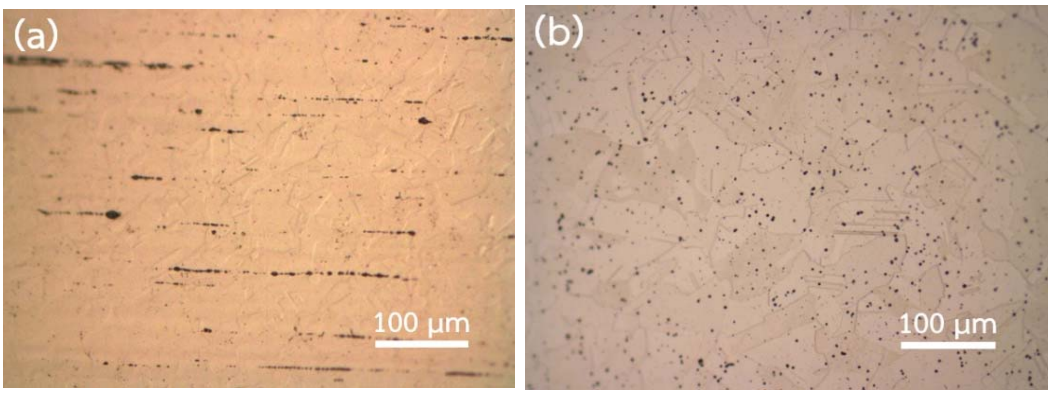

Figure 4. Metallography of as-quenched specimen indicating a) elongated inclusions on the longitudinal plane b) globular shape inclusions on the transversal plane.

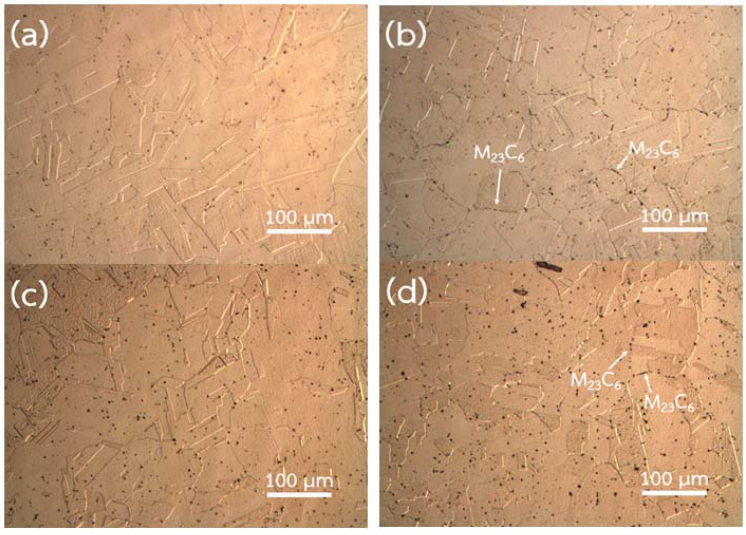

Figure 5. Microstructures after aging of solution treated specimen a) A, b) B, c) C, and d) D.

Figure 5 shows each specimen microstructure developed as a result of predetermined aging conditions. Longer annealing time and higher aging temperature on B and D resulted in larger averaged grain size with the presence of second phase particles at GBs. The particles were primarily identified as carbides by selective electro-etching using Oxalic acid on bulk substrates. Electron micrograph of their up-closed appearance was presented in Figure 6 for morphological examination and EDX analysis. The latter compounds to analytic verification of the second phase along GBs as $M_{23}C_6$ which composed majorly of Cr.

σ-phase is also a major phase but of intermetallic types in high Cr-content (25-30 wt. %) austenitic SS whereas other phases, including η- and χ-phase, are considered minor [9]. σ-phase emerges in Cr-rich δ-ferrite regions during aging in a temperature range of 600-1000°C [11-12]. When precipitated, its brittle character stands out and bring about hardness increment and toughness decrement of the materials [13]. Due to the fact that less hardness value of sample D than that of sample C was measured, this phenomenon releases σ-phase responsibility from the basis strengthen mechanism just mentioned and thus it hardly forms. Spruiell [8] found that its formation only enhances in cold worked steels. This implies strengthening mechanism of our steels is controlled only by $M_{23}C_6$ dispersion instead of other second phases and this gives an explanation of measured hardness value in Figure 7.

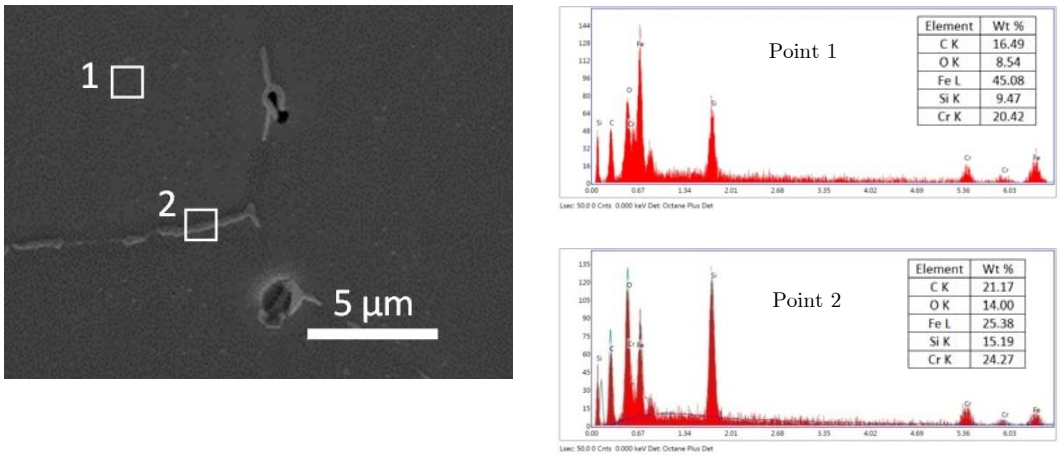

Figure 6. Electron micrographs of solution treated specimen B along with EDX results.

It is well established that mechanical properties are influenced by characters of developing precipitation during aging. At first, small clusters of $M_{23}C_6$ rapidly nucleate at GBs but scarcely inside grains. Their effectiveness to hinder dislocation is relatively ineffective in this incipient stage which results in the lowest strength in sample A. Strengthening continues in samples B and C with growing precipitates scattering evenly during aging. Too long exposure at higher temperature accelerates carbide coarsening and grain growing resulting in strength reduction of sample D.

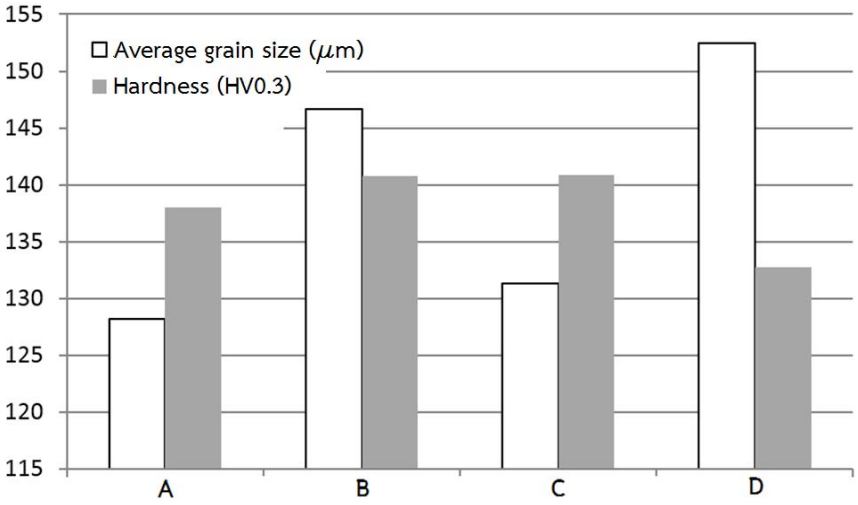

Figure 7. Average grain size (μm) and hardness values (HV0.3) of each specimens.

3.2 Carbonaceous Deposit

Figure 8 and 9 indicate carbonaceous yields and their corresponding schematic diagrams of different morphology under SEM investigation on each experimental substrate. Two distinct regions, i.e. intergranular and intragranular, could be identified in the figures. In the former region are disconnected straight bundles of the CNTs (Figure 8a, 8b and at higher magnification Figure 9). Directional orientation of each bundle toward a junction supports intergranular locations where carbides preferably precipitated (Figure 6). Even through twin boundaries are naturally abundant in the austenitic steels (Figure 5), no structure of the bundles is detected resembling to the twin boundary (Figure 8). This coincides with the fact that there were no carbides observed along coherent twin boundaries. The findings are interpreted as a relevant evidence that during CVD process GBs with the presence of carbides are the reactive areas which is thereby carbide controlled process of CNT synthesis.

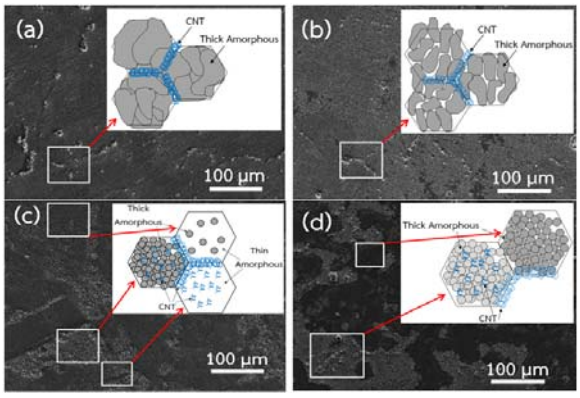

Figure 8. Carbon nanostructure characteristics and their schematic morphology on substrates a) A, b) B, c) C, and d) D.

In general, the formation of carbonaceous deposits on metallic substrates through CVD follows a two-step mechanism. The first step is a dissociation of a carbon containing gas on catalyst nanoparticles into elementary carbons which then diffuse on or dissolves in relevant matrix domains. When thermodynamically and kinetically conditions are satisfied, various allotropes of carbon precipitate through decomposition or precipitation processes [14]. Similar mechanism occurs in case of metal dusting of which three main active mechanisms were proposed [15-16]. As in our case, the process becomes two folds more complicated when (1) ethanol vapor was used as the primary carbon source and (2) 316L SS alloy as bulk catalytic substrates. At high temperature environment, ethanol molecular of ethanol undergo thermal cracking into many intermediate reactive reagents and the most likely intermediates are free radial hydrocarbon and etching hydroxide reagent OH^- [17-19]. The hydrocarbon, an acting secondary carbon source, will catalysis-enhanced thermally dissociates into free carbon and hydrogen atoms. This completes the second step when the carbon atoms segregate into a carbon nanostructure.

Based on the fact that CNT nucleate and grow intergranularly (Figure 8), catalytic role of phases present at the GB should be recognized. Before the carbonaceous growth starts, carbide formation within GBs during pre-aging leaves adjacent region Cr-depleted or Fe-Ni rich. This introduces two catalytic candidates, i.e. $M_{23}C_6$ particles and Fe-Ni rich phase. Empty d-shell in the Fe-Ni phase is known to facilitate hydrocarbon decomposition over $M_{23}C_6$. Free carbons, as a result, dissolve and diffuse into the transition metal matrix and graphite subsequently segregates when carbon content exceeds solubility limit [15-16]. However, the CNT found at GB in all samples indicates otherwise. It is suspected that the free and excess carbons from Cr-depleted zone aggregate at intergranular $M_{23}C_6$ instead and then induce a famous tip/root growth mechanism of the CNTs. The other possibility is that $M_{23}C_6$ could directly disintegrate into CNT and metallic particles. However, this is not the case since the carbides is relatively stable at low oxygen partial pressure and is unlikely to disintegrate in our experimental condition.

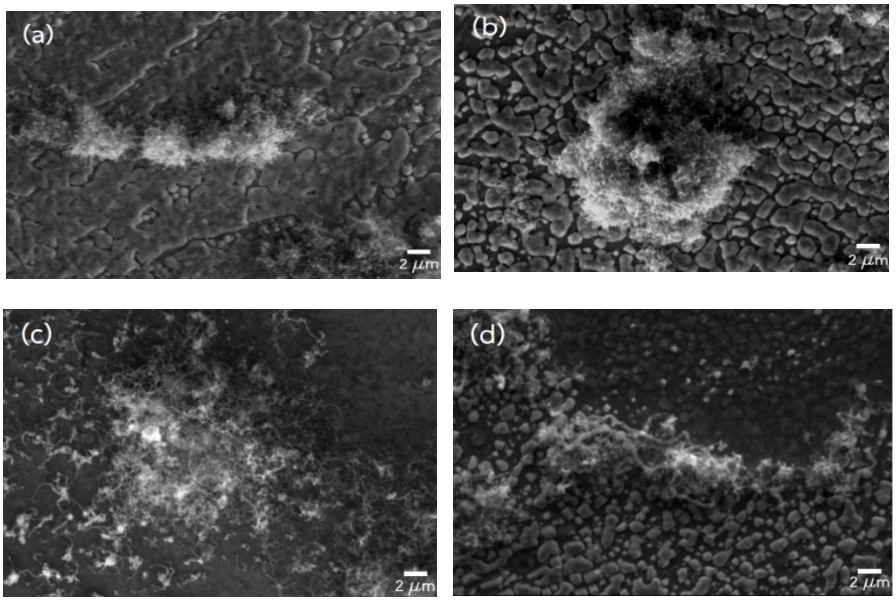

Figure 9. Scanning electron micrograph of (a,b) Disconnected CNT bundles with carbonaceous aligned intergranular with thick amorphous carbonaceous deposit in D

For intragranular observation, large thick plates of amorphous carbon deposit are clearly seen in sample A (Figure 9a) but appeared smaller in sample B (Figure 9b). Because chromia layers, the protective films covering SS, is reduced during annealing at 700°C before CVD process, gaseous decomposition could occur all over the fresh surface. The carbon deposition is resembles to coke formation on low carbon steels that cooperate aggregation of free carbon atoms and disintegration of Fe_3C into amorphous carbon on their surfaces. The difference in size of the carbon islands may be as a result of precipitation extent of Fe_3C which distributes more uniformly in sample A than in B. This leads to microstructural homogeneity of Fe_3C producing unfavorable CNT formation sites in sample A. In sample C (Figure 9c) and D (Figure 9d) which are subjected to higher aging temperature, small thick amorphous carbon plates with and without CNTs and short CNT on substrate surfaces are observed. The condition accelerates σ-phase formation to a level enough to alter CNT formation mechanism but not enough to change substrate mechanical properties. Unfortunately, since σ-phase particles is so small during nucleation stage that both SEM and hardness measurement could not detect their influence but published TTP diagram indicates otherwise. However, σ-phase during nucleation stage could be verified further using TEM.

4. Conclusions

Microstructural effects of 316L substrates on CNT synthesis through CVD are examined in this experiment. Given four microstructural substrates distinguished by precipitate characters yield different morphology of carbonaceous deposits. Results show that CNTs do not grow haphazardly on all the samples but favorably locate where carbide of type $M_{23}C_6$ presents. Catalytic roles of Fe-Ni rich phase for gaseous decomposition at GBs was proposed while intergranular carbides nearby served as a function of CNT nucleation and growth sites where decomposed carbons segregate. The latter mechanism agrees with the famous top/bottom growth of CNTs when exothermic decomposition of the hydrocarbon in Fe-Ni phase enhance local endothermic of CNT precipitation at nearby $M_{23}C_6$. This makes the carbide a favor location for such the top/bottom mechanism to take place. Nevertheless, amorphous carbonaceous deposit dominated intragranularly. It is believed that the controlling mechanism is as the same case as coke formation mechanism in which coke, amorphous carbonaceous deposit, creates directly from decomposition Fe_3C. When microstructural alteration was produced by σ-phase formation after aged at higher temperature, morphology of carbon deposits changes. This validates microstructural effects of substrates.

The search of the most effective way to fabricate hybrid nano-metallic components in field emission or supercapacitor applications has led to a direct growth of CNTs on metallic substrates. Large scale production of the CNTs on metallic substrates from ethanol vapor is advantageous regarding to lower production temperature. When the effect of microstructure of substrates is expressed in this research, microstructural initialization of substrates should not be negligent. Precipitation occurring during synthesizing time can alter carbonaceous deposit formation mechanism; thus, the concerns of substrate degradation and reuse. Manipulating substrates' microstructure could be essential for homogeneity and selective growth of CNTs.

5. Acknowledgments

We would like to express our sincere gratitude to the financial supporters, the Thailand Graduate Institute of Science and Technology (TGIST) No. TG-55-22-55-043M of the National Science and Technology Development Agency (NSTDA) and the Higher Education Research Promotion (HERP) of the Office of the Higher Education Commission (OHEC).

References

[1] Bhushan, B., **2007.** Handbook of Nanotechnology, Springer, New York.

[2] J.M. Bonard, J.P. Salvetat, T. Stockli, L. Forro, and A. Chatelain., **1999.** Field emission from carbon nanotubes: perspectives for application and clues to the emission mechanism, Applied Physics A, 69, 245-254.

[3] Gao, L., Peng, A., Wang, Z.Y. and Zhang, H., **2008.** Growth of aligned carbon nanotube arrays on metallic substrate and its application ot supercapacitors, Solid State Communications, 146, 380-383.

[4] Hiraoka, T., Yamada, T. and Hata, K., **2006.** Synthesis of single- and double-walled carbon nanotube forests on conducting metal foils, *Journal of the American Chemical Society*, 128, 13338-13339.

[5] Ghrobani, H., Rashidi, A. M., Rastegari, S., Mirdamadi, S. and Alaei, M., **2001.** Mass production of multi-wall carbon nanotubes by metal dusting process with high yield, Materials Research Bulletin, 46, 716-721.

[6] Camilli, L., Scarselli, M., Gobbo, S.D., Castrucci, P., Nanni, F., Gautron, E., Lefrant, S. and Crescenzi, M.D., **2011.** The synthesis and characterization of carbon nanotubes grown by chemical vapor deposition using a stainless steel catalyst, Carbon, 49, 3307-3315.

[7] ASTM Internationation, **2011.** Wesr Conshohocken, PA, USA.

[8] Spruiell, J.E., Scott, J.A., Ary, C.S. and Hardin, R.L., **1973.** Microstructural stability of thermal-mechanically pretreated type 316 austenitic stainless steel, Metallurgical Transactions, 4, 1533-1544.

[9] Marshall, P., **1984.** Austenitic Stainless Steels, Microstructure and Mechanical properties, Elsevier.

[10] Weiss, B. and Strickler, R., **1972.** Phase instabilities during high temperature exposure of 316 austenitic stainless steel, Metallurgical Transactions, 3, 851-866.

[11] Waanders, F.B., Vorster, S.W. and Pollak, H., **1999.** The influence of temperature on σ-phase formation and the resulting hardening of Fe-Cr-Mo-alloys, Hyperfine Interactions, 120-121, 751-755.

[12] Peckner, D. and Bernstein, I.M., **1977.** Handbook of Stainless Steels, 1st edition ed., McGraw-Hil, New York, USA.

[13] Lee, J., Kim, I. and Kimura, A., **2003.** Journal of Nuclear Science and Technology, 40, 664-671.

[14] Seah, C.M., Chai, S.P. and Mohamed, A.R., **2011.** Synthesis of aligned carbon nanotubes, Carbon, 49, 4613-4635.

[15] Szakalos, P., Pettersson, R. and Hertzman, S., **2002.** An active corrosion mechanism for metal dusting on 304L stainless steel, Corrosion Science, 44, 2253-2270.

[16] Szakalos, P., **2004.** Mechanisms of metal dusting, Department of Materials Science and Engineering, Royal Institute of Technoogy.

[17] Maruyama, S., Kolima, R., Miyauchi, Y., Chiashi, S. and Kohno, M., **2002.** Low-temperature synthesis of high-purity single-walled carbon nanotubes from alcohol, Chemical Physics Letters, 360, 229-234.

[18] Murakami, Y., Miyauchi, Y., Chiashi, S. and Maruyama, S., **2003.** Characterization of single-walled carbon nanotubes catalytically synthesized from alcohol, Chemical Physics Letters, 374, 53-58.

[19] Murakami, Y., Chiashi, S., Miyauchi, Y., Hu, M., Ogura, M., Okubo, T. and Maruyama, S., **2003.** Growth of vertically aligned single-walled carbon nanotube films on quartz substrates and their optical anitropy, Chenical Physics Letters, 385, 298-303.